Computers and Concrete, *Vol. 18, No. 4 (2016) 853-876*
DOI: http://dx.doi.org/10.12989/cac.2016.18.4.853

Plastic hinge characteristics of RC rectangular columns with Fiber Reinforced Polymer (FRP)

B. Mohebi[*1], S.M. Hosseinifard[1a] and M. Bastami[2b]

[1]*Faculty of Engineering, Imam Khomeini International University, Qazvin, Iran*
[2]*International Institute of Seismology and Earthquake Engineering, Tehran, Iran*

(Received November 16, 2014, Revised May 1, 2016, Accepted May 17, 2016)

Abstract. This study is based on extending the previous research work entitled Fiber reinforced polymers (FRP) confined columns that published by the authors. The modeling characteristics for plastic hinges of RC columns have been determined in FEMA 356. However, for evaluating a retrofitted member, there are no parameters for one. This issue is an important deficiency of the mentioned code. The main purpose of this study is to introduce the plastic hinge parameters for the RC rectangular columns that are retrofitted by FRP. These characteristics of plastic hinges can be used in a nonlinear static analysis, instead of nonlinear dynamic one. In order to analytical simulation of RC column behavior and also accuracy of acquired results, at first using LS-DYNA software including 3D nonlinear finite element modeling, a RC column studied in the literature has been verified. The obtained results are showed a good match between both Finite element model and experimental test and there are reasonable correlations between ones. Moreover in the next stage, in order to evaluate the robustness of the proposed method 20 reinforced concrete columns which supposed to be fixed at one end, have been retrofitted using FRP in the plastic hinge zone. The columns have been simulated under a constant compressive load and lateral cyclic displacement that the hysteresis curves have been drawn for obtaining the plastic hinge parameters. Numerical results demonstrate that the plastic hinge parameters have averagely been increased after retrofitting with a thickness of CFRP about 0.165 mm.

Keywords: FRP; RC column; plastic hinge; retrofitting; cyclic loading; finite element analysis

1. Introduction

Most of the existing structures in high earthquake risk areas don't meet the requirements of recent earthquake codes and subsequently lead to structural failure by earthquakes. Most failures of the RC buildings in earthquakes are related to the failure of columns. The main reasons for these failures can be ascribed to the shear failure of columns, loss of concrete columns in bottom areas, inadequate length of reinforcement overlap at the foot of the columns and buckling of column bars. Lateral confinement of the existing reinforced concrete columns can significantly

[*]Corresponding author, Assistant Professor, E-mail: mohebi@eng.ikiu.ac.ir
[a]Ph.D. student, E-mail: maryamhosseinifard@edu.ikiu.ac.ir
[b]Associate Professor, E-mail: m.bastami@iiees.ac.ir

http://www.techno-press.org/?journal=cac&subpage=8 ISSN: 1598-8198 (Print), 1598-818X (Online)

increase their lateral deflection capability and load bearing capacity. As a result, different methods have been proposed for strengthening of plastic hinge zones of columns, which among ones, fiber reinforced polymer (FRP) composites have some advantages and are used successfully and extensively for seismic performance improvement. Warping FRP around reinforced concrete columns is a proved method in retrofitting structures to resist against earthquakes. A numerical study on concrete cubic and cylinder confined with FRP has been performed by Malvar *et al.* (2004). The results showed an increase in resistance of the models and also this model confirmed that circular sections indicate more confinement than rectangular sections. A non-linear finite element analysis under combined axial and lateral cyclic loads on a circular reinforced concrete columns covered with FRP has been done by Parvin and Wang (2002). They observed that the column's strength and plasticity in the area which suffer from plastic joints were increased. Another investigation by Promis *et al.* (2009) was related to strengthening of short reinforced concrete columns with FRP under a combination of compression and bending. The other research on one-fifth scale reinforced concrete bridge columns by Saadatmanesh *et al*. (1996 & 1997) showed that the FRP jacket can also be applied to enhance the performance of the reinforced concrete bridge columns under constant axial load and lateral cyclic loading. Their research illustrated that the FRP jacket effectively prevents from bond failure or longitudinal bar buckling of columns. Realfonzo ***et al.*** (2009) performed a wide experimental test to evaluate the seismic performance of RC columns which externally confined with fiber-reinforced polymers (FRPs). Their specimens consisted of full scale square columns, 300 mm on each side, subjected to a constant axial load and monotonic or cyclic flexure. They investigated the benefits of some strengthening systems in terms of strength, ductility, and energy dissipation capacity .Recent research by De Luca *et al*. (2011) is an experimental test on full-scale square and rectangular reinforced concrete columns externally confined with glass and basalt-glass FRP laminates and subjected to pure axial load .The study has been conducted to investigate how the external confinement effects on peak axial strength and deformation of a prismatic reinforced concrete column. The results have been shown that the FRP confinement increases the concrete axial strength but it is more effective in enhancing of the concrete strain capacity. Xiao and Ma (1997) investigated a prefabricated composite jacketed system to retrofit of the reinforced concrete columns with lap-spliced rebars. They concluded that the FRP jacket delay the premature brittle failure of columns due to the bond deterioration of the lap-spliced rebars. Xiao and Wu (2000) experimentally investigated that the most influential parameters affecting on the behavior of FRP confined concrete are compressive strength and confinement modulus. They also proposed a simple bilinear stress–strain model for confined concrete which was claimed to be in good agreement with the experimental results from previous studies. Spoelstra and Monti (1999) presented an uniaxial analytical model for FRP-confined concrete. Their study pointed out the differences in the behaviors of concrete elements confined with a variety of wraps such as fiberglass or carbon fiber. They also derived some relations between axial and lateral strains to trace the state of strain or detect its failure mode. Seible *et al.* (1997) validated the seismic design of reinforced concrete columns retrofitted using carbon fiber through large-scale bridge column experiments and determined that carbon fiber jackets provide the desired inelastic design deformation capacity levels as well as steel shell jacketing. Ilki *et al.* **(**2008) have been represented a detailed study of several parameters which affect on columns with CFRP sheets. Thickness of the CFRP jacket, cross-section shape, concrete strength, amount of internal transverse reinforcement, corner radius, existence of predamage, loading type (monotonic or cyclic) and the bonding pattern (orientation, spacing, anchorage details, additional corner supports) of CFRP sheets were the main test parameters of Ilki *et al.*'s experimental work. Test results showed that external confinement of columns with CFRP sheets leads to an increase in ultimate strength and ductility. Samaan *et al.* (1998) proposed a simple analytical confined model to predict the response of FRP-confined concrete. They validated this analytical model through their own experiments as well as the ones by others and observed good correlation between the analytical and experimental results. Parvin and Wang (2001) investigated the behavior of FRP-jacketed square concrete columns under eccentric loading both experimentally and numerically. Their results demonstrated that the strength and ductility of concrete FRP-jacketed columns under eccentric loading can substantially increase and as well the strain gradient decrease the retrofitting efficiency of the FRP jacket for concrete columns. The similar study has been performed to evaluate nonlinear parameters of FRP confined circular columns for bridge piers by Ghodrati Amiri *et al.* (2012). It's noted that, FRP strengthening techniques are not limited to reinforced concrete columns. Ludovico *et al.* (2007) have been considered a retrofitting method using glass fiber-reinforced polymer (GFRP) on a full-scale three-story framed structure. They compared the theoretical results with the experimental outcomes to assess the effectiveness of the proposed retrofitted technique and also validation of the adopted design procedures. They considered design assumptions and criteria along with nonlinear static pushover analysis to evaluate the overall capacity of the FRP-retrofitted structure. Furthermore, Karayannis *et al.* **(**2008) experimentally have been investigated the behavior of critical external beam–column joints repaired or/and strengthened with CFRP sheets. Their study have been represented that the combination of this technique with the use of CFRP sheets leads to a significant improvement of the loading capacity, the energy absorption and the ductility.

2. Background theory

2.1 Stress-strain models

Concrete confinement is an efficient technique for increasing the load-carrying capacity and ductility of RC columns. Investigations done by researchers have determined different models to predict the ultimate strength and stress-strain curve of FRP-confined rectangular sections. Some of these models can be named as Mander *et al.*'s stress-strain model that is based on presented formula in 1973 as

$$\varepsilon_{cc} = \varepsilon_{co}\left[1+5\left(\frac{f_{cc}'}{f_{co}'}-1\right)\right] \tag{1}$$

where f_{co}', ε_{co}, f_{cc}' and ε_{cc} are compressive strength, the corresponding strain of the unconfined concrete, peak confined concrete stress and the corresponding strain, respectively.

In 2001, Lam and Teng also performed experimental tests on rectangular and square concrete samples covered with FRP. In this model the effective surface area (A_e/A_c) is provided as

$$\frac{A_e}{A_c} = \frac{1-\left[(b/h)(b-2R_c)^2+(h/b)(b-2R_c)^2\right]/(3A_g)-\rho_{sc}}{1-\rho_{sc}} \tag{2}$$

where A_e, A_c and A_g are the cross-sectional area of effectively confined concrete section, the cross-sectional area surrounding with FRP and the gross area of concrete section, respectively. *b* and *h* are the width and height of a member and R_c is the radius of edges of a prismatic cross section confined with FRP; The parameter ρ_{sc} is the ratio of longitudinal steel reinforcement area to cross-sectional area of the member (*As* /*bh*).

Shape coefficient (k_s) and equivalent cover pressure (f_1) are obtained from following relations

$$k_s = \frac{b}{h}\frac{A_e}{A_c} \tag{3}$$

$$f_l = \frac{2f_{frp}t_{frp}}{\sqrt{h^2+b^2}} \tag{4}$$

where f_{frp} and t_{frp} are tensile strength and thickness of one ply of the FRP sheets, respectively.

Strength of retrofitted rectangular concrete columns using the above values can be obtained from the following equation

$$\frac{f_{cc}'}{f_{co}'} = 1 + k_1 k_s \frac{f_l}{f_{co}'} \tag{5}$$

where k_1 is the efficiency factor of FRP coverage which has been determined from experimental tests for different shapes.

ACI 440 Committee (2008) has presented a compressive strength versus ultimate axial strain for RC rectangular columns with FRP based on the arch action of confined rectangular concrete. Moreover, effective confinement coefficient has been defined as

$$k_e = \frac{A_e}{A_c} = 1 - \frac{(b-2r)^2 (d-2r)^2}{3A_g(1-\rho_{sg})} \tag{6}$$

where *b* and *d* are dimensions of the column, *r* is the radius of the corners and ρ_{sg} is the longitudinal steel reinforcement ratio.

Compressive strength f_{cc}' and ultimate axial strain of confined concrete ε_{cu} are provided from the Eqs.(7)-(8)

$$k_e = \frac{A_e}{A_c} = 1 - \frac{(b-2r)^2 (d-2r)^2}{3A_g(1-\rho_{sg})} \tag{6}$$

where *b* and *d* are dimensions of the column, *r* is the radius of the corners and ρ_{sg} is the longitudinal steel reinforcement ratio.

Compressive strength f_{cc}' and ultimate axial strain of confined concrete ε_{cu} are provided from the Eqs.(7)-(8)

$$\frac{f_{cc}'}{f_{co}'} = -1.254 + 2.254\sqrt{1+\frac{7.94 f_l}{f_{co}'}} - 2\frac{f_l}{f_{co}'} \tag{7}$$

$$\varepsilon_{cu} = \frac{1.71\left(5f'_{cc} - 4f'_{co}\right)}{E_c} \tag{8}$$

where f_l is confining pressure due to FRP jacket, E_c is the modulus of elasticity of concrete and other parameters has already been defined.

2.2 Ductility of retrofitted columns under bending

Columns are retrofitted to increase the plasticity and also depreciate the seismic energy before occurrence of the failure modes. Ductility coefficient based on displacement that states the ductility of the structure can be written as

$$\mu_\Delta = \frac{\Delta_u}{\Delta_y} \tag{9}$$

where Δ_u and Δ_y are ultimate displacement and yielding displacement, respectively.
According to Park's studies in1989, ultimate displacement will occur when the load is reduced to 20% of maximum load or when reinforcement bars fail. The curve ductility coefficient ϕ_u that was used by Priestly *et al.* (1996) can be expressed as

$$\mu_\phi = \frac{\phi_u}{\phi_y} \tag{10}$$

where ϕ_y and ϕ_u are curve coefficients at the first yielding moment and ultimate limit, respectively. Next, plastic displacement $\left(\Delta_p\right)$ and the coefficient of plastic curve $\left(\phi_p\right)$ are defined as

$$\Delta_p = \Delta_u - \Delta_y \tag{11}$$

$$\phi_p = \phi_u - \phi_y \tag{12}$$

Coefficient of plastic curve $\left(\phi_p\right)$ is assumed to be constant in the plastic hinge. The relation between displacement ductility and ductility coefficient of the curve is expressed as

$$\mu_\Delta = 1 + 3\left(\mu_\phi - 1\right)\frac{L_p}{L}\left(1 - 0.5\frac{L_p}{L}\right) \tag{13}$$

L is the shear zone length and L_p is the plastic hinge zone length which can be obtained as

$$L_p = 0.08L + 0.022 f_{yl} d_{bl} \geq 0.044 f_{yl} d_{bl} \tag{14}$$

where f_{yl} and d_{bl} are yield strength and diameter of longitudinal bars, respectively. Plastic rotation $\left(\theta_p\right)$ is obtained through multiplying plastic hinge length by the coefficient of plastic curve

$$\theta_p = L_p \phi_p \tag{15}$$

Many researchers use these relations to obtain the hysteresis curves. It has been shown that the FRP wrapping considerably increases the ductility of column against the earthquake forces. In

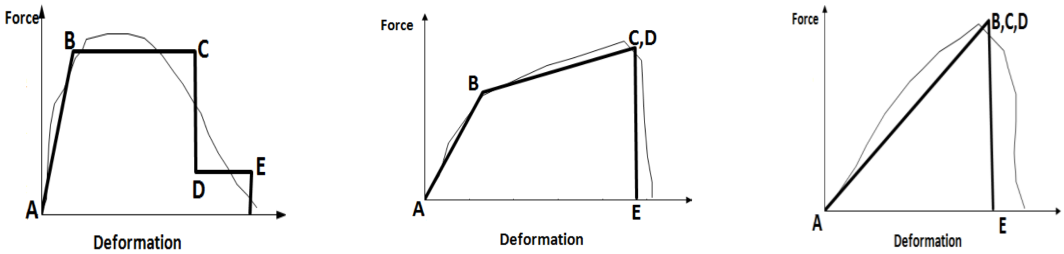

(a) (b) (c)

displacement controlled force controlled

Fig. 1 Force- displacement curves in (a) ductile, (b) Semi-ductile and (c) brittle manner (FEMA 440, 2005)

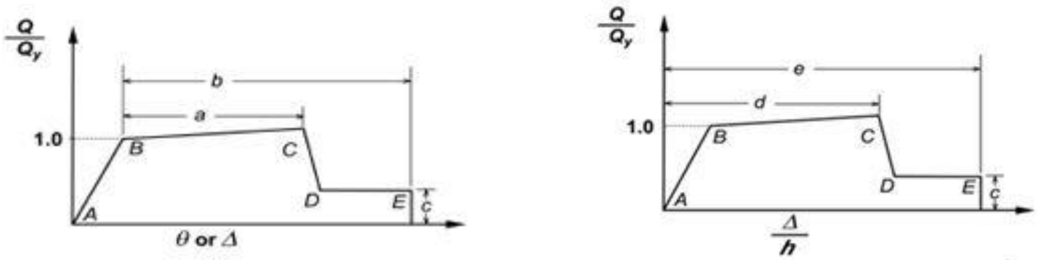

(a) (b)

Fig. 2 Generalized force-deformation relations for concrete elements or components (a) Deformation and (b) Deformation ratio (FEMA 356, 2000)

concrete columns with inadequate transverse stirrups, increasing the ductility coefficient (μ_Δ) due to the flexural deformation to 2.5~3.5 is very difficult because the ultimate strain of non-coverage concrete is very low, whereas using FRP cover much greater ductility can be achieved, i.e. $\mu_\Delta > 6$.

2.3 Pushover analysis

Total capacity of a structure depends on the strength and displacement capacities of each member. To achieve the structure capacity in an elastic region, a nonlinear analysis such as pushover analysis should be used. In fact, this method is a nonlinear static analysis and lateral forces have been gradually increased until the members yield and ultimately the structure becomes unstable. The capacity curves consist of two axes having base shear (vertical) versus roof lateral displacement at mass center of the structure as target displacement (horizontal). These curves which form the basis of nonlinear static procedures are discussed below. They are generated by subjecting a detailed structural model to one or more lateral load patterns (vectors) and then increasing the magnitude of the total load to generate a nonlinear inelastic force-deformation relationship for the structure at a global level (FEMA 440, 2005).

Table 1 Modeling parameters and numerical acceptance criteria for nonlinear procedures-reinforced concrete columns (FEMA 356, 2000)

Conditions			Modeling parameters[2]			Acceptance criteria[2]				
			Plastic rotation angle, radians		Residual strength ratio	Plastic rotation angle, radians				
						Performance level				
						IO	Component type			
							Primary		Secondary	
			a	b	c		LS	CP	LS	CP
Columns controlled by flexure										
$P/(A_g f'_c)$	Trans. Reinf.[1]	3.77 V/(b.d)/ f'c								
≤0.1	C	≤3	0.02	0.03	0.2	0.005	0.015	0.02	0.02	0.03
≤0.1	C	≥6	0.016	0.024	0.2	0.005	0.012	0.016	0.016	0.024
≥0.4	C	≤3	0.015	0.025	0.2	0.003	0.012	0.015	0.018	0.025
≥0.4	C	≥6	0.012	0.02	0.2	0.003	0.01	0.012	0.013	0.02
≤0.1	NC	≤3	0.006	0.015	0.2	0.005	0.005	0.006	0.01	0.015
≤0.1	NC	≥6	0.005	0.012	0.2	0.005	0.004	0.005	0.008	0.012
≥0.4	NC	≤3	0.003	0.01	0.2	0.002	0.002	0.003	0.006	0.01
≥0.4	NC	≥6	0.002	0.008	0.2	0.002	0.002	0.002	0.005	0.008

1. "C" and "NC" are abbreviations for conforming and nonconforming transverse reinforcement. A component is confining if within the flexural plastic hinge region, hoops are spaced at ≤d/3, an, if, for components of moderate and high ductility demand. The strength provided by the hoops (V_S) is at least three- fourths of the design shear. Otherwise the component is considered nonconforming.
2. Linear interpolation between values listed in the table shall be permitted.

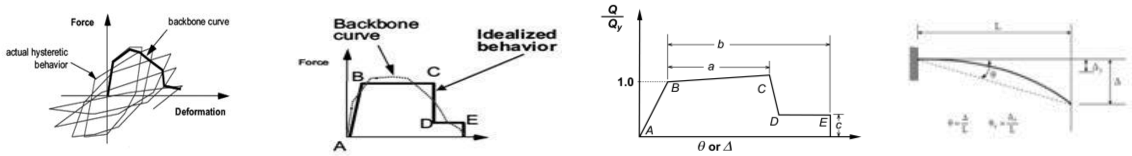

(a) (b) (c) (d)

Fig. 3 Obtaining plastic hinge parameters(a) Backbone representation of hysteretic behavior (FEMA 440, 2005) (b) Idealizing push of hysteresis curve(FEMA 440, 2005) (c) Generalized force-deformation relations for concrete elements or components(FEMA 356, 2000) (d) Definition of rotation or (FEMA 356, 2000)

2.3.1 Behavior of structural members

Behavior of structural members with regards to the force-displacement curve subjected to applied loads divides to two categories as force or displacement controlled. Force-displacement curves have been presented in three different parts including ductile, semi-ductile and brittle manners as shown in Fig. 1.

2.3.2 Modeling parameters and numerical acceptance criteria for nonlinear procedures-reinforced concrete columns

In this section, modeling parameters for RC members based on FEMA 356 are explained. In these codes, force-displacement curves have been considered as shown in Fig. 2.

(a) Deformation, or Type I. In this curve, deformations are expressed directly using terms such as strain, curvature, rotation, or elongation. Parameters *a* and *b* refer to those portions of the deformation that occur after yielding; i.e. plastic deformation. Parameter *c* is reduced resistance after sudden reduction from *C* to *D*. Parameters *a*, *b* and *c* are defined numerically in various tables in this chapter. Alternatively, parameters *a*, *b* and *c* should be allowed to be directly determined by the analytical procedures justified by experimental evidence.

(b) Deformation ratio, or Type II. In this curve, deformations are expressed in terms such as shear angle and tangential drift ratio. Parameters *d* and *e* refer to total deformations measured from the origin. Parameters *c*, *d* and *e* are defined numerically in various tables in this chapter. Alternatively, parameters *c*, *d* and *e* should be allowed to be directly determined by the analytical procedures justified by experimental evidence (FEMA 356, 2000).

2.3.3 Plastic hinge characteristics in columns

Plastic hinge characteristics of reinforced concrete columns depend on shear and axial force, dimension of section, compressive strength of concrete and transverse reinforcement. These values have been presented in Table 1.

2.3.4 Obtaining plastic hinge parameters

It is necessary to cite an appropriate procedure to gain plastic hinge parameters from hysteresis curves. Force-displacement and moment-rotation hysteresis curves should be obtained for each model through modeling and analyzing the columns. Then, according to FEMA 440 instructions the push curves of moment-rotation hysteresis curves are drawn (Fig. 3(a)) and, push curves are idealized so that the area under the push of the idealized curve fit to the area under the push of hysteresis curve (Fig. 3(b)). Finally, plastic hinge parameters are determined using idealized curves as shown in Fig. 3(c). It should be mentioned that in one fixed end members θ is total amount of elastic and plastic rotation (Fig. 3(d)).

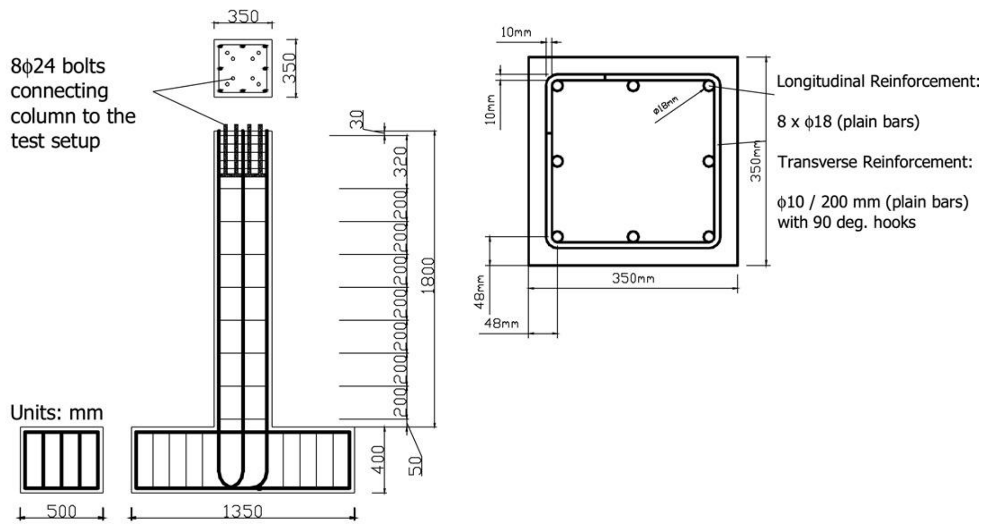

Fig. 4 Details of test specimens (Ozcana *et al*. 2008)

Table 2 Details of test specimens (Ozcana *et al*. 2008)

Specimen	Specimen properties				Longitudinal steel ratio (%)	Axial load level *N/N0*(%)	CFRP Implementation	
	f_c (Mpa)	f_y (Mpa)	Reinforcement				Ply No.	Strengthening
			Longitudinal	Transverse				
S-NL-0-34	14					34	0	Reference
S-NL-1-27	19.4					27	1	NL
S-UL-1-34	14	287	8 18 mm (plain bars)	10-mm diameter bars at 200 mm	1.66	34	1	UL
S-NL-2-39	11.4					39	2	NL
S-UL-2-32	15.6					32	2	UL

3. Experimental work for verification

An experimentally work has been done by Ozcana *et al*. (2007) on the RC rectangular columns strengthened with FRP sheets in plastic hinge zone (50 cm from the bottom of columns). Details of test specimens are shown in Fig. 4 and Table 2.

4. Finite element analysis of FRP-jacketed columns

In this investigation finite element method has been used to analyze of the column models. LS-DYNA_971 is suitable software for nonlinear analysis that employs finite element method to analyze engineering problems. In the following finite element modeling of concrete, steel and FRP will be expressed.

4.1 Elements

Eight nodes hexahedral solid element has been used for concrete modeling. This element with three translational degrees of freedom in each node has the capability of being cracked and considers the plastic deformations. The geometry and position of nodes of solid element have been shown in Fig. 5.

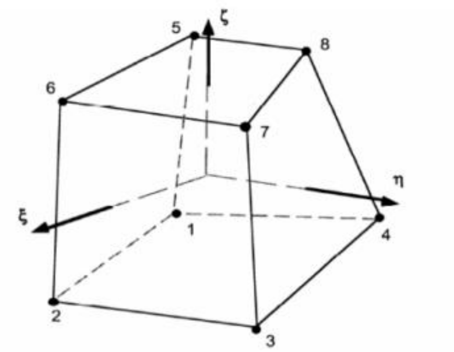

Fig. 5 Eight nodes solid hexahedron element (LS-DYNA 2007)

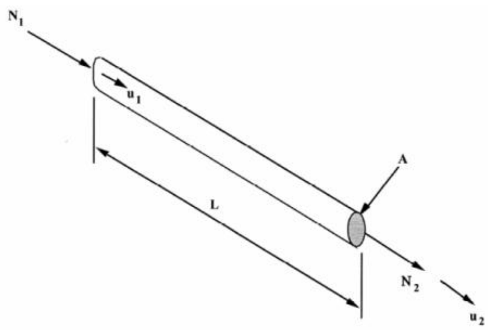

Fig. 6 Truss element (LS-DYNA 2007)

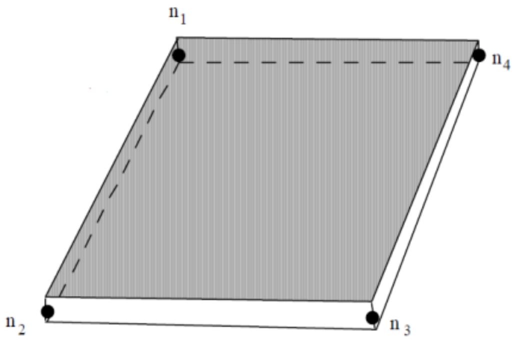

Fig. 7 Shell element (LS-DYNA 2007)

Two nodes truss elements has been applied for steel bars, as shown in Fig.6. This element has three degrees of freedom at each node and carries an axial force. Two constitutive models are implemented for truss element: elastic and elastic-plastic with kinematic hardening (LS-DYNA 2007).

As shown in Fig. 7, four nodes two-dimensional shell elements have been used to model FRP layers. The thickness of elements can be specified. For orthotropic and anisotropic composites a local material angle can be defined as well. Moreover, Chang-Chang composite failure model can aptly simulate the failure modes of FRP layer. Five material parameters have been used in cracking, compression and fiber breakage failure criteria (LS-DYNA, 2007).

4.2 Material properties

Properties of concrete, steel and CFRP are presented in Tables 1, 2 and 3, respectively. Winfrith-concrete model which has been applied for concrete materials is a smeared crack model that can be used in the elements with eight integration points. Plastic-kinematic model is one of the LS_DYNA material models which consider kinematic and isotropic hardening. Thus, this model is convenient for steel rebars under cyclic loading. Moreover, composite-damage model has been used to simulate FRP sheets; this model has a brittle failure behavior. In the experimental works homemade CFRP anchorages have been placed along the retrofitted region of the columns to achieve good connection between the column and CFRP sheet. In order to apply these carbon fiber anchor dowels, formed by carbon fiber strips in a rolled shape, some holes were drilled between

Table 3 Properties of concrete

Density	Modulus of elasticity	Compressive strength	Tensile strength (Column)	Poisson ratio
2400 Kg/m3	20000 MPa	28 MPa	3.2 MPa	0.2

Table 4 Properties of steel

Density	Modulus of elasticity	Yield stress (Column)	Poisson ratio
7800 Kg/m3	200000 MPa	420 MPa	0.3

Table 5 Properties of CFRP

Density	Thickness of each layer	Poisson ratio	Shear modulus	Transverse Compressive strength	Transverse Tensile strength	Longitudinal Tensile strength	Shear strength	Modulus of elasticity in transverse direction	Modulus of elasticity in longitudinal direction	Thickness of each layer
1820 Kg/m3	0.165 mm	0.3	3400 MPa	540 MPa	540 MPa	3500 MPa	676 MPa	3e3 MPa	230e3 MPa	0.165 mm

two longitudinal bars. The anchorages were placed to prevent debonding of CFRP sheets during the test. These dowels can also be used for seismic retrofitting of rectangular RC columns with FRP wrapping to enhance confinement efficiency. As a result, FRP sheets have been considered full connected to concrete columns of finite element model.

4.3 Specimen

In this research 20 reinforced concrete columns have been retrofitted using FRP. All the columns have been supposed to be fixed at one end and having 2 m height. The FRP sheet has also been applied to bottommost 0.5 m of the column in the plastic hinge zone.

4.4 Loading pattern

The columns have been simulated under a constant compressive load and lateral cyclic displacement similar to the seismic loading. In all the models the axial load has been applied before starting the lateral loading. A foundation with the dimensions 400×600×1400 mm having

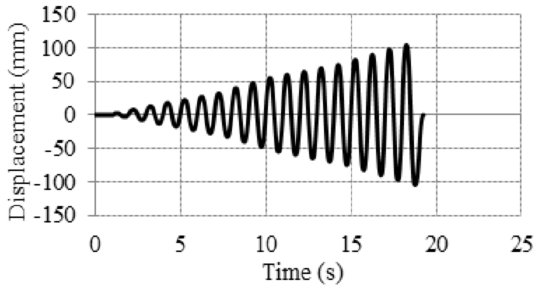

Fig. 8 Loading pattern applied to columns (Perera 2006)

Table 6 Dimensions of column model

Model No.	Transverse Reinforcement	Pn/Ag.f'c		3.77 Vn/b.d.√f'c		b*h (cm)	Reinforcement	
							Longitudinal	Transverse
1	C	≤0.1	0.1	≥6	6	40*60	12Φ36	Φ12@14cm
2	C		0.1		7		12Φ40	Φ12@12cm
3	C		0.05		6.5		12Φ36	Φ12@14cm
4	C	≥0.4	0.4	≥6	6		12Φ35	Φ12@14cm
5	C		0.4		7		12Φ39	Φ12@12cm
6	C		0.7		6.5		12Φ40	Φ12@14cm
7	NC	≤0.1	0.1	≤3	3	35*35	8Φ28	Φ10@28cm
8	NC		0.1		2		8Φ22	-
9	NC		0.05		3		8Φ27	Φ10@28cm
10	NC		0.05		2		8Φ22	-
11	NC	≤0.1	0.1	≥6	6	40*60	12Φ36	Φ14@22cm
12	NC		0.1		7		12Φ40	Φ14@22cm
13	NC		0.05		6.5		12Φ36	Φ14@22cm
14	NC	≥0.4	0.4	≤3	3	35*35	8Φ28	Φ10@28cm
15	NC		0.4		2		8Φ19	-
16	NC		0.7		3		8Φ32	Φ10@28cm
17	NC		0.7		2		8Φ25	-
18	NC	≥0.4	0.4	≥6	6	40*60	12Φ35	Φ14@22cm
19	NC		0.4		7		12Φ39	Φ14@22cm
20	NC		0.7		6.5		12Φ40	Φ14@22cm

fix end condition has been embedded at the bottom of the column. Furthermore, a similar concrete part has been modeled at the top of the column to prevent concentrated stresses. Lateral cyclic displacement has been selected according to many references which have been studied the behavior of concrete columns experimentally. In this study displacement per cycle has been increased with a drift increment about 0.5% (Fig. 8).

4.5 Dimensions of columns

Dimensions of the columns are demonstrated in Table 6. According to FEMA 356 C and NC are abbreviations for conforming and nonconforming transverse reinforcements, respectively. In fact, these criteria show the transverse confinement of members.

5. Validating the results of finite element analysis

In numerical studies, calibration of software results is a necessary step to achieve reliable

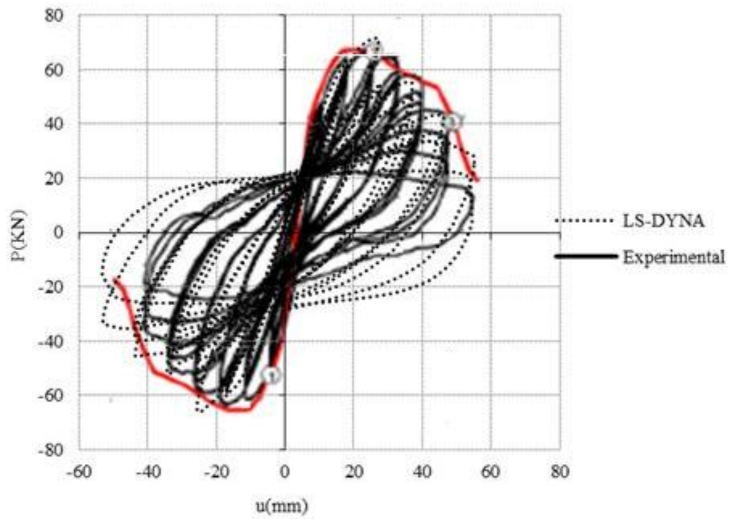

Fig. 9 Comparison experimental and numerical force-displacement hysteresis of column without FRP

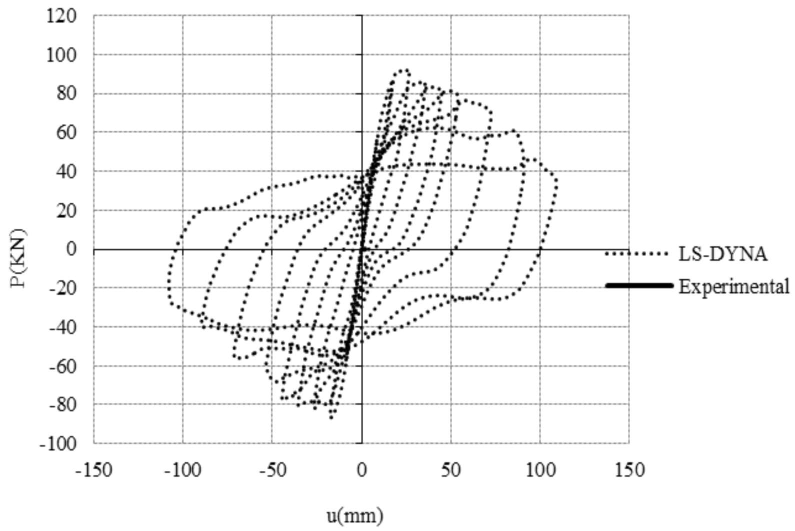

Fig. 10 Comparison experimental and numerical force-displacement hysteresis of column with FRP

outcomes. Thus, our first priority is to compare the acquired results via finite element model with an experimental test results. The experimental tests have been performed by Ozcana *et al.* (2008) on rectangular reinforced concrete columns. Two examples of reinforced concrete columns have been modeled including with and without FRP retrofitting in plastic hinge area. Both columns have been subjected to compressive axial force and lateral cyclic displacement. Then, hysteresis curves have been obtained using base shear force and the displacement at the top of the column.

As presented in Figs. 9 and 10, the comparison results between the experimental and finite element models are shown acceptable compliance.

Another verification approach has also been adopted in order to increase our confidence of the accuracy of numerical method which causes to obtain plastic hinge parameters of reinforced

Table 7 Dimensions of column models

Model	b×h,mm	f'c, Mpa	fy(bar), Mpa	fy(tie), Mpa	Reinforcement Longitudinal	Reinforcement Transverse	Axial load,N
2-NO FRP	400×600	28	420	280	12Φ36	Φ12@14cm	672000
3-NO FRP	400×600	28	420	280	12Φ37	Φ12@14cm	336000
4-NO FRP	400×600	28	420	280	12Φ36	Φ14@22cm	672002
5-NO FRP	350×350	28	420	280	8Φ28	Φ10@28cm	1372000

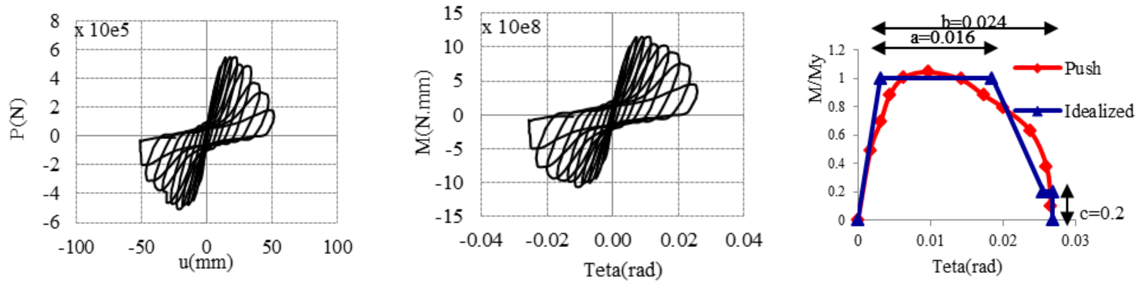

(a) (b) (c)

Fig. 11 Hysteresis curves of column model 2-NO FRP (a) Force-Displacement hysteresis curve, (b) Moment-rotation hysteresis curve and (c) Push and idealized curves

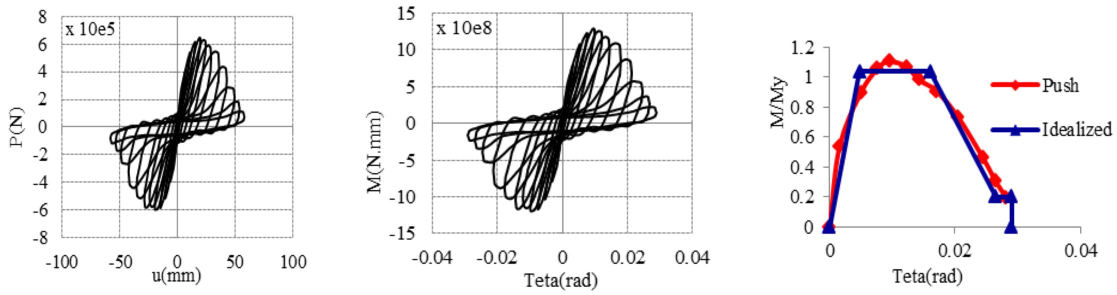

(a) (b) (c)

Fig. 12 Hysteresis curves of column model 3-NO FRP (a) Force-Displacement hysteresis curve, (b) Moment-rotation hysteresis curve and (c) Push and idealized curves.

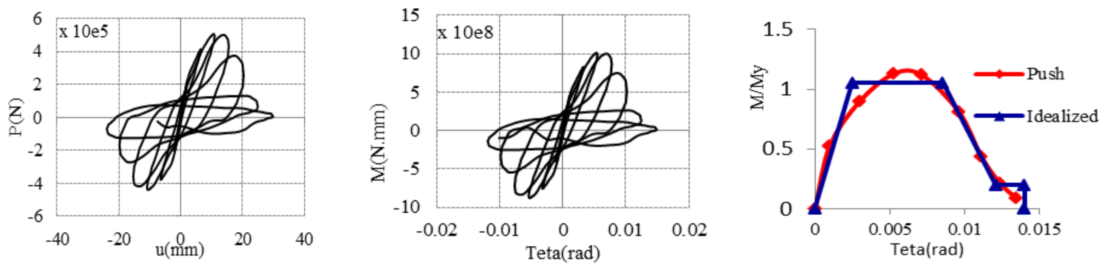

(a) (b) (c)

Fig. 13 Hysteresis curves of column model 4-NO FRP (a) Force-Displacement hysteresis curve, (b) Moment-rotation hysteresis curve and (c) Push and idealized curves

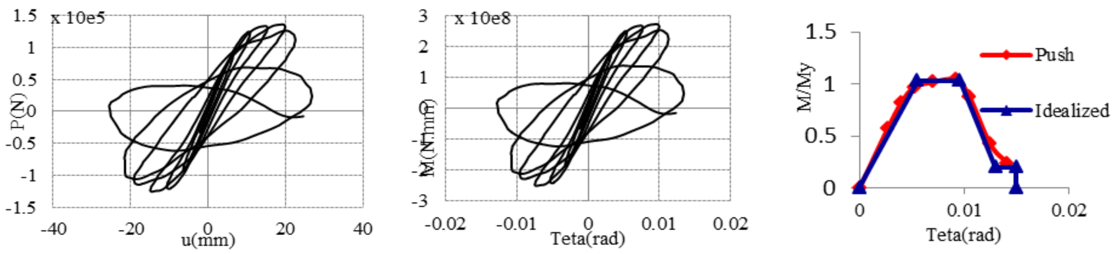

(a) (b) (c)

Fig. 14 Hysteresis curves of column model 5-NO FRP (a) Force-Displacement hysteresis curve (b) Moment-rotation hysteresis curve (c) Push and idealized curves

Table 8 Comparison between the results of analysis and FEMA 356 in columns without FRP

Model	3.77 Vn/b.d.√f'c	Pn/Ag .f'c	Modeling parameter values presented in FEMA 356			Modeling parameter values obtained from analysis		
			Plastic rotation angle, radians		Residual strength ratio	Plastic rotation angle, radians		Residual strength ratio
			a	b	c	a	b	c
2-NO FRP	6	0.1	0.016	0.024	0.2	0.016	0.024	0.2
3-NO FRP	6	0.4	0.012	0.02	0.2	0.0113	0.0242	0.2
4-NO FRP	6	0.1	0.005	0.012	0.2	0.0061	0.012	0.2
5-NO FRP	3	0.4	0.003	0.01	0.2	0.0041	0.0097	0.2

concrete columns available in FEMA 356. To gain this purpose, four concrete columns have been designed using ACI code criteria according to the second, fourth, sixth and seventh rows of Table 1 as demonstrated in Table 7.

Force-displacement hysteresis curves have been achieved from finite element analysis in order to find plastic hinge parameters using FEMA 440 instructions. This process has completely been shown in Figs. 11-14. In resumption, plastic hinge parameters extracted from the analysis have been compared with similar values given by FEMA 356 which are shown acceptable conformity as presented in Table 8. The amount of plastic hinge parameters of analysis has shown acceptable conformity. As a result, the finite element model has been confirmed to be useful along with the aims of the current study.

7. The modeling results

The columns have been modeled and analyzed then force-displacement and moment-rotation curves have been obtained by the software. Hysteresis curves for column model No.1 have been shown in Figs. 15(a)-(b) then push and idealized curve of hysteresis curve drawn in Fig. 15(c). Hysteresis curves of the other columns have been presented in appendix.

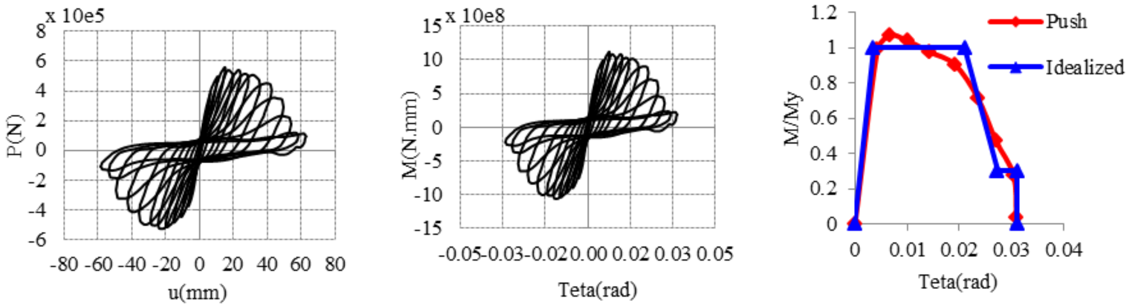

(a) (b) (c)

Fig. 15 Hysteresis curves of column model No.1 (a) Force-Displacement hysteresis curve, (b) Mome rotation hysteresis curve and (c) Push and idealized curves.

Table 9 Plastic hinge characteristics of retrofitted columns

Model No.	Transverse Reinforcement	Pn/Ag.f'c	3.77 Vn/b.d.√f'c	Parameters		
				Plastic Shear Angle, radians		Residual Strength Ratio
				a	b	c
1	C	0.1	6	0.0175	0.0276	0.3
2	C	0.1	7	0.0163	0.0253	0.35
3	C	0.05	6.5	0.0178	0.0278	0.3
4	C	0.4	6	0.0139	0.0244	0.35
5	C	0.4	7	0.0125	0.0233	0.3
6	C	0.7	6.5	0.0124	0.0234	0.3
7	NC	0.1	3	0.0094	0.0155	0.3
8	NC	0.1	2	0.0119	0.017	0.25
9	NC	0.05	3	0.0097	0.0171	0.25
10	NC	0.05	2	0.0149	0.0224	0.25
11	NC	0.1	6	0.0075	0.0136	0.3
12	NC	0.1	7	0.0052	0.0127	0.3
13	NC	0.05	6.5	0.0067	0.0129	0.31
14	NC	0.4	3	0.0065	0.0106	0.22
15	NC	0.4	2	0.0068	0.012	0.21
16	NC	0.7	3	0.0045	0.01	0.2
17	NC	0.7	2	0.0047	0.0102	0.26
18	NC	0.4	6	0.0053	0.0107	0.35
19	NC	0.4	7	0.0041	0.0106	0.31
20	NC	0.7	6.5	0.0043	0.0083	0.33

8. Conclusion

In this paper, evaluating a retrofitted member using FRP in order to achieve the plastic hinge parameters has been investigated. For this, at first the sample columns have been simulated and analyzed by the software then force-displacement, moment-rotation hysteresis curves and plastic hinge characteristics through hysteresis curves have been obtained. Moreover, in the next stage in order to confidence of the robustness and also accuracy of the proposed numerical method, an experimental work has been verified. These values have been presented in Table 9. Considering hysteresis curves and comparing plastic hinge parameters of the columns before and after retrofitting with a thickness of CFRP about 0.165 mm are shown an increase in the 20 column models averagely. Based on the numerical studies, the following results can be concluded:

• The value of parameter **a** and **b** have been increased up to 59% and 14%, respectively. Furthermore, the value of parameter **c** which represents the residual strength ratio in most models has been increased from 0.2 in the columns without FRP to 0.3 in retrofitted columns.

• As shown, increasing the value of parameter **a** in the columns due to strengthening method is more than parameter **b**. This indicates that retrofitting procedure is more effective in ductility than strength of columns after the occurrence of maximum moment.

• The ultimate displacement in retrofitting rectangular columns that have been warped with CFRP layers considerably increases. Hysteresis curves have also been shown a suitable increase in energy absorption capacity and ductility, but it's should be noted that this kind of retrofitting has not significant influence on shear capacity.

• Increasing the axial load of columns leads to a reduction in plastic hinge parameters and consequently, columns fail in a brittle manner.

• As can be observed in the acquired results, retrofitting RC columns with FRP cause to an increase in the value of plastic hinge parameters. These characteristics of plastic hinges can be used in a nonlinear static analysis for retrofitted members instead of dynamic one.

References

ACI 440 Committee State of the Art Report on FRP for Concrete Structures (ACI 440R-96) (1996), *Manual of concrete Practice*, American Concrete Institute, Farmington with Hills, Michigan, pp.68.

De Luca, A., Nardone, F., Matta, F., Nanni, A., Lignola, G. and Prota, A. (2011), "Structural evaluation of full-scale FRP-confined reinforced concrete columns", *J. Compos. Constr.,* **15**(1), 112-123.

Di Ludovico, M., Prota, A., Manfredi, G. and Cosenza, E. (2007), "Seismic strengthening of an under-designed RC structure with FRP", John Wiley & Sons, Ltd., **37**(1), 141-162.

FEMA 356, Applied Technology Council (2000), "Pre standard and commentary for the seismic rehabilitation of buildings", Federal emergency management agency, Washington.

FEMA 440, Applied Technology Council (ATC-55 Project) (2005), "Improvement of nonlinear static seismic analysis procedures", Washington, Federal emergency management agency.

Ghodrati Amiri, G., Jaberi Jahromi, A. and Mohebi, B. (2012), "Determination of plastic hinge properties for static nonlinear analysis of FRP-strengthened circular columns in bridges", *Comput. Concr.,* **10**(5), 435-455.

Ilki, A., Peker, O., Karamuk, E., Demir, C. and Kumbasar, N. (2008), "FRP retrofit of low and medium strength circular and rectangular reinforced concrete columns", *J. Mater. Civ. Eng.,* **20**(2), 169-188.

Karayannis, C. and Sirkelis, G. (2008), "Strengthening and rehabilitation of RC beam-column joints using carbon-FRP jacketing and epoxy resin injection", John Wiley & Sons, Ltd., **37**(5), 769-790.

Lam, L. and Teng, J.G. (2001), "FRP-confined rectangular concrete columns", *J. Struct. Eng.*

LS-DYNA Keyword Users Manual (version 971) , May 2007.

Malvar, L.J., Morrill, B.K. and Crawford, E.J. (2004), "Numerical modeling of concrete by fiber-reinforced composites", *J. Compos. Constr.*, **8**(4), 315-322.

Mander, J.B., Priestly, M.J.N. and Park, R. (1988), "Theoritical stress-strain model for confined concrete", *J.*

Struct. Eng., **114**(8), 1804-1826.
Ozcana, O., Binici, B. and Ozcebe, G. (2008), "Improving seismic performance of deficient reinforced concrete columns using carbon fiber-reinforced polymers", *J. Eng. Struct.*, **30**(6), 1632-1646.
Parvin, A. and Wang, W. (2002), "Concrete columns confined by fiber composite warps under combined axial and cyclic lateral loads", *J. Compos. Struct.*, **58**(4), 539-549.
Perera, R. (2006), "A numerical model to study the seismic retrofit of RC columns with advanced composite jacketing", *Compos. Part B: Eng.*, **37**(4), 337-345.
Promis, G., Ferrier, E. and Hamelin, P. (2009), "Effect of external FRP retrofitting on reinforced concrete short columns for seismic strengthening", *J. Compos. Struct.*, **88**(3), 367-379.
Realfonzo, R. and Napoli, A. (2009), "Cyclic behavior of RC columns strengthened by FRP and steel devices", *J. Struct. Eng.*, **135**(10), 1164-1176.
Saadatmanesh, H., Ehsani, M.R. and Jin, L. (1996), "Seismic strengthening of circular bridge pier models with fiber composites", *ACI Struct. J.*, **93**(6), 639-47.
Saadatmanesh, H., Ehsani, M.R. and Jin, L. (1997), "Seismic retrofitting of rectangular concrete columns retrofitted with composite straps", *Earthq. Eng. Res. Inst. J. SPECTRA*, **13**(2), 281-304.
Samaan, M., Mirmiran, A. and Shahawy, M. (1998), "Model of concrete confined by fiber composites", *J. Struct. Eng.*, **124**(9), 1025-31.
Seible, F., Priestley, M.J.N., Hegemier, G.A. and Innamorato, D. (1997), "Seismic retrofit of RC columns with continuous carbon fiber jackets", *J. Compos. Constr.*, **1**(2), 52-62.
Spoelstra, M. and Monti, G. (1999), "FRP-confined concrete model", *J. Compos. Constr. ASCE*, **3**(3), 143-50.
Xiao, Y. and Ma, R. (1997), "Seismic retrofit of RC circular columns using prefabricated composite jacketing", *J. Struct. Eng.*, **123**(10), 1357-64.
Xiao, Y. and Wu, H. (2000), "Compressive behavior of concrete confined by carbon fiber composite jackets", *J. Mat. Civil Eng.*, **12**(2), 139-46.

CC

Appendix

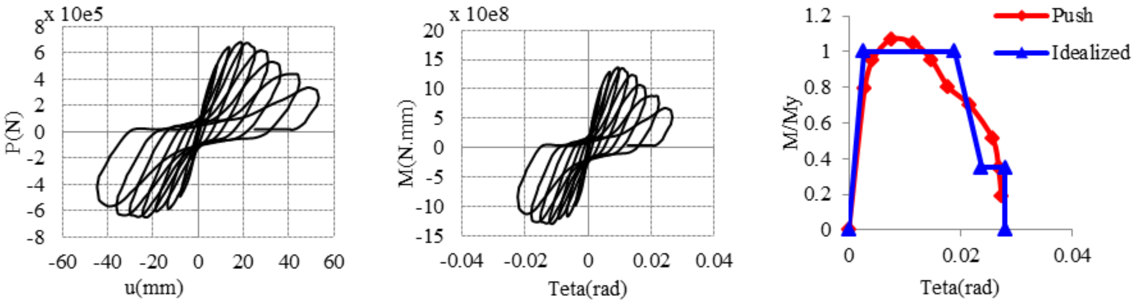

(a) (b) (c)

Fig. 1 Hysteresis curves of column model No.2 (a) Force-Displacement hysteresis curve, (b) Moment-rotation hysteresis curve and (c) Push and idealized curves

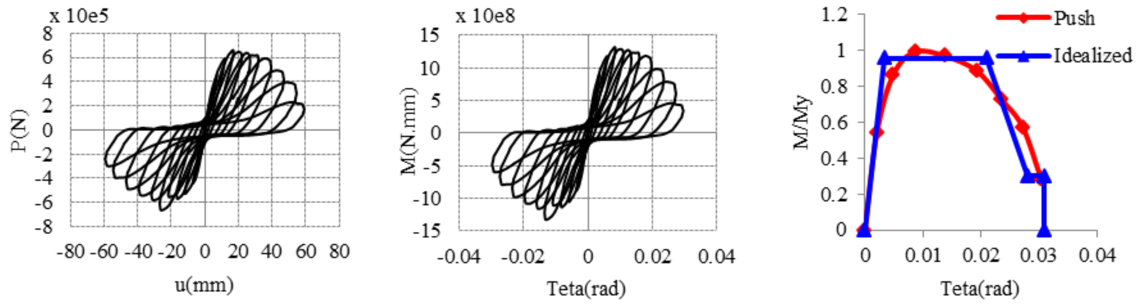

(a) (b) (c)

Fig. 2 Hysteresis curves of column model No.3 (a) Force-Displacement hysteresis curve, (b) Moment-rotation hysteresis curve and (c) Push and idealized curves

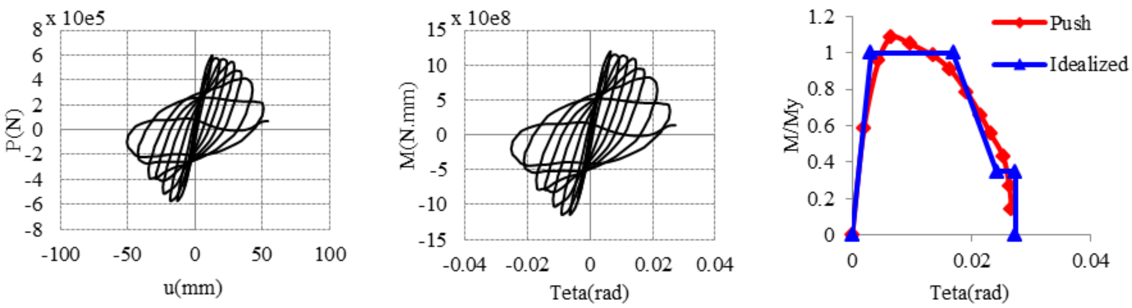

(a) (b) (c)

Fig. 3 Hysteresis curves of column model No.4 (a) Force-Displacement hysteresis curve, (b) Moment-rotation hysteresis curve and (c) Push and idealized curves

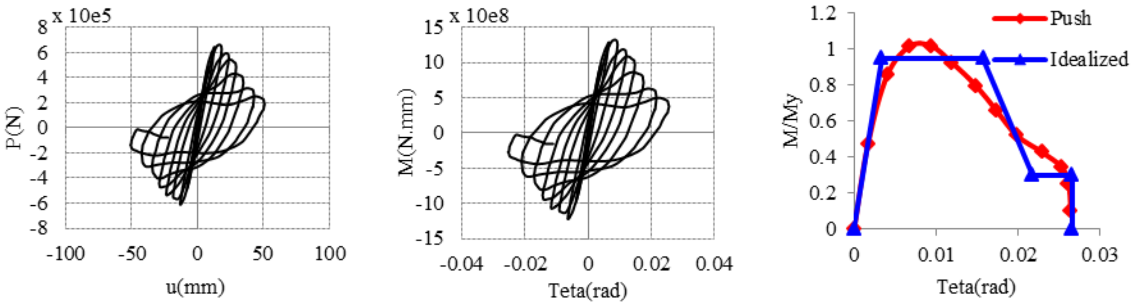

(a) (b) (c)

Fig. 4 Hysteresis curves of column model No.5 (a) Force-Displacement hysteresis curve, (b) Moment-rotation hysteresis curve and (c) Push and idealized curves

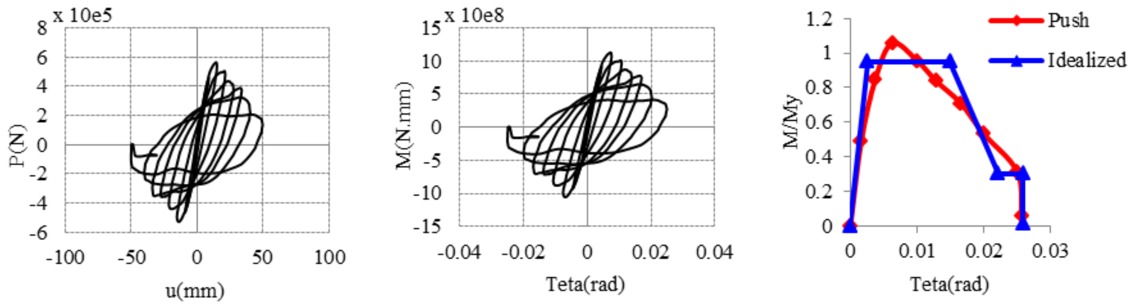

(a) (b) (c)

Fig. 5 Hysteresis curves of column model NO.6 (a) Force-Displacement hysteresis curve, (b) Moment-rotation hysteresis curve and (c) Push and idealized curves

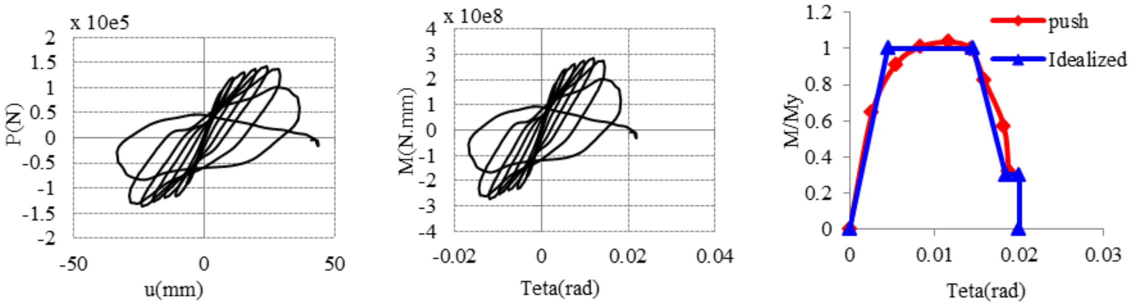

(a) (b) (c)

Fig. 6 Hysteresis curves of column model No.7 (a) Force-Displacement hysteresis curve, (b) Moment-rotation hysteresis curve and (c) Push and idealized curves.

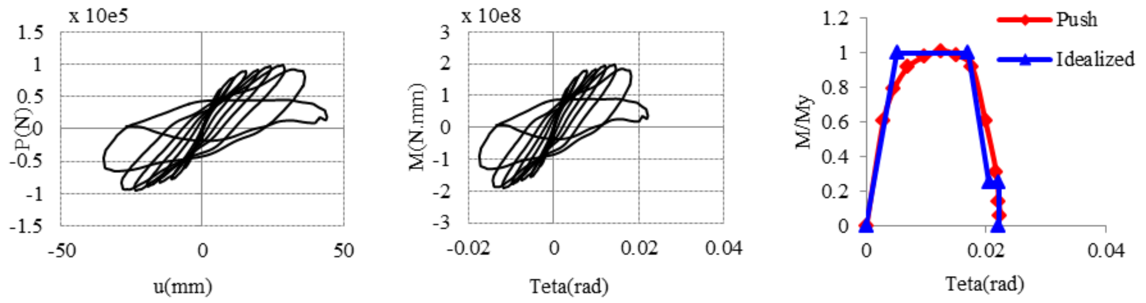

(a) (b) (c)

Fig. 7 Hysteresis curves of column model No.8 (a) Force-Displacement hysteresis curve, (b) Moment-rotation hysteresis curve and (c) Push and idealized curves

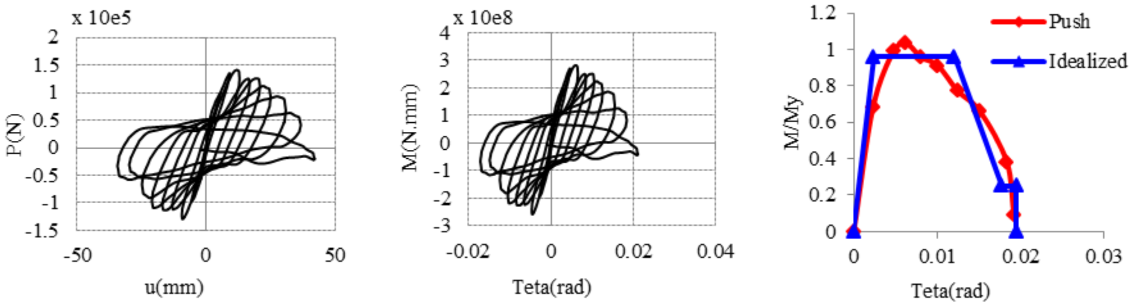

(a) (b) (c)

Fig. 8 Hysteresis curves of column model No.9 (a) Force-Displacement hysteresis curve, (b) Moment-rotation hysteresis curve and (c) Push and idealized curves

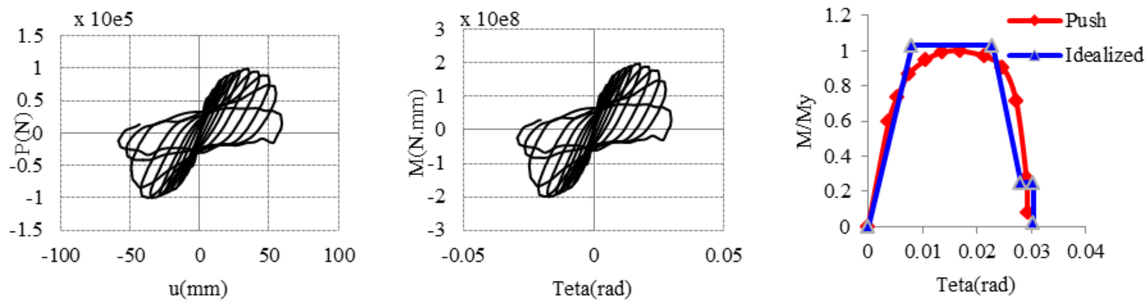

(a) (b) (c)

Fig. 9 Hysteresis curves of column model No.10 (a) Force-Displacement hysteresis curve, (b) Moment-rotation hysteresis curve and (c) Push and idealized curves

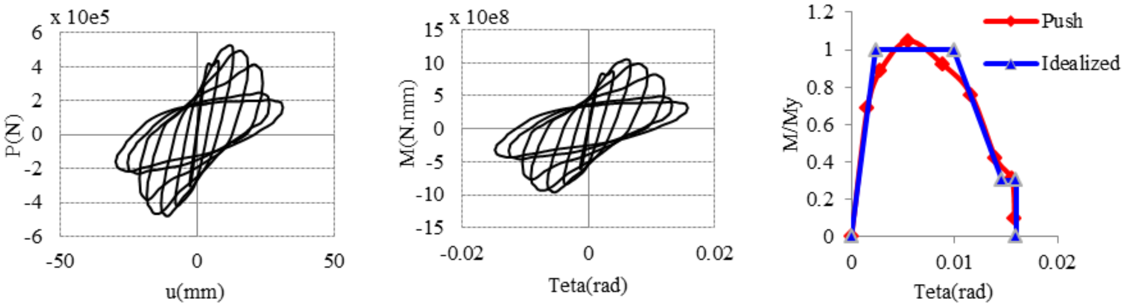

(a) (b) (c)

Fig. 10 Hysteresis curves of column model No.11 (a) Force-Displacement hysteresis curve, (b) Moment-rotation hysteresis curve and (c) Push and idealized curves

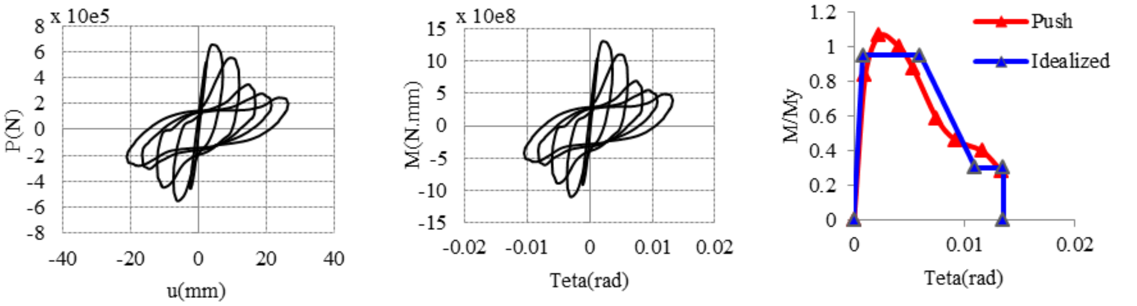

(a) (b) (c)

Fig. 11 Hysteresis curves of column model No.12 (a) Force-Displacement hysteresis curve, (b) Moment-rotation hysteresis curve and (c) Push and idealized curves

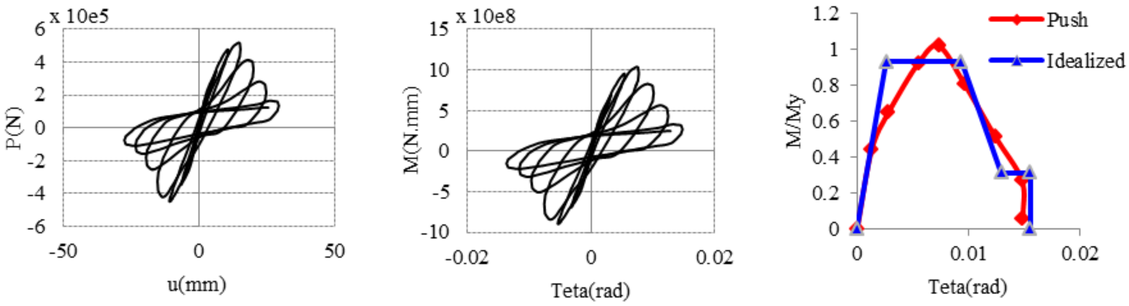

(a) (b) (c)

Fig. 12 Hysteresis curves of column model No.13 (a) Force-Displacement hysteresis curve, (b) Moment-rotation hysteresis curve and (c) Push and idealized curves

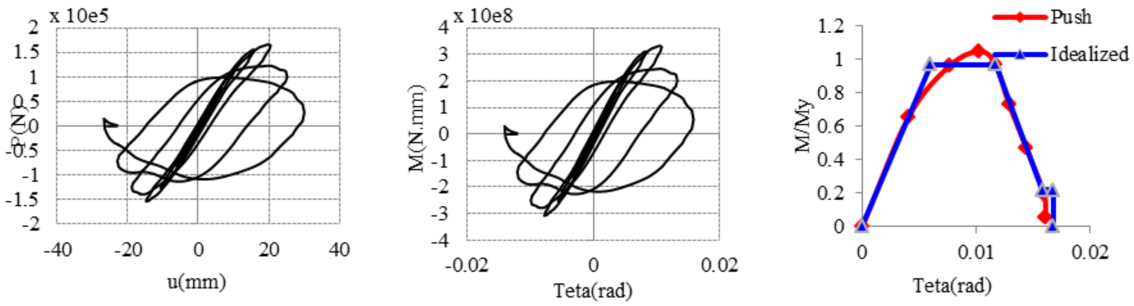

(a) (b) (c)

Fig. 13 Hysteresis curves of column model No.14 (a) Force-Displacement hysteresis curve, (b) Moment-rotation hysteresis curve and (c) Push and idealized curves

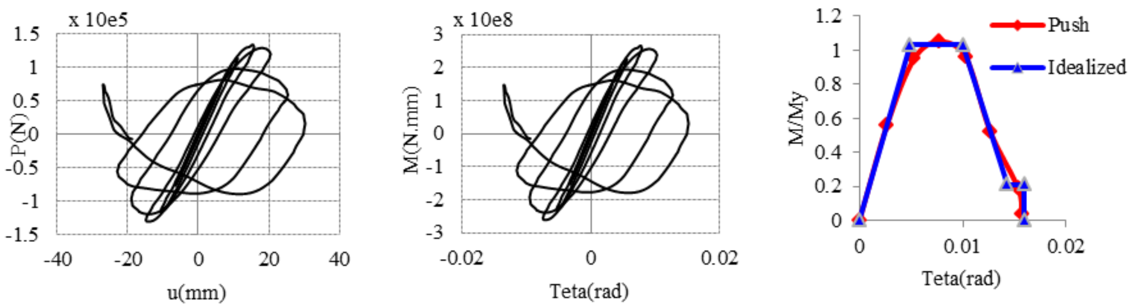

(a) (b) (c)

Fig. 14 Hysteresis curves of column model No.15 (a) Force-Displacement hysteresis curve, (b) Moment-rotation hysteresis curve and (c) Push and idealized curves

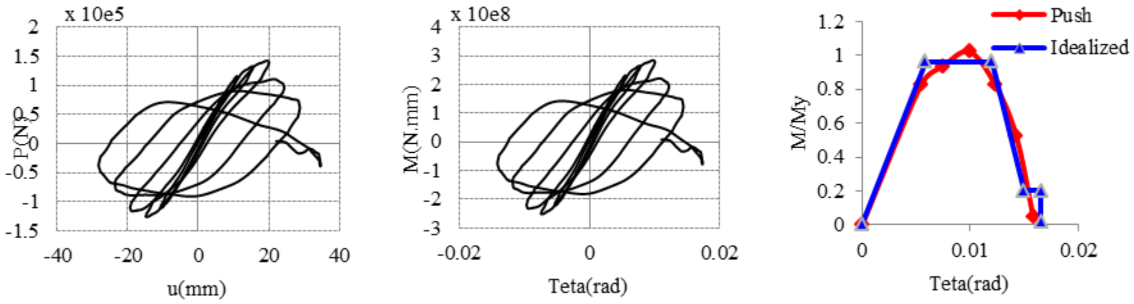

(a) (b) (c)

Fig. 15 Hysteresis curves of column model No.16 (a) Force-Displacement hysteresis curve, (b) Moment-rotation hysteresis curve and (c) Push and idealized curves

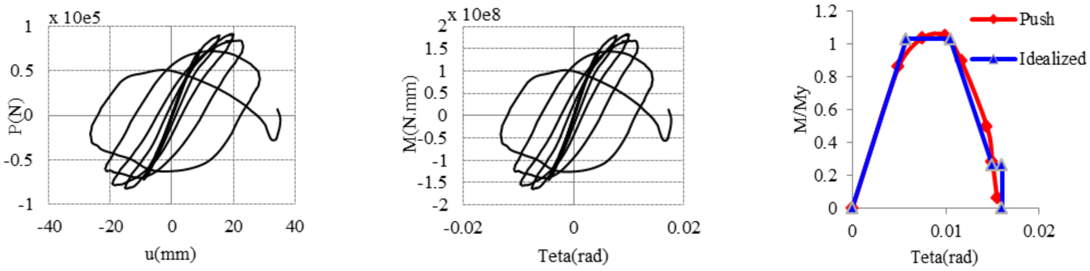

(a) (b) (c)

Fig. 16 Hysteresis curves of column model No.17 (a) Force-Displacement hysteresis curve, (b) Moment-rotation hysteresis curve and (c) Push and idealized curves

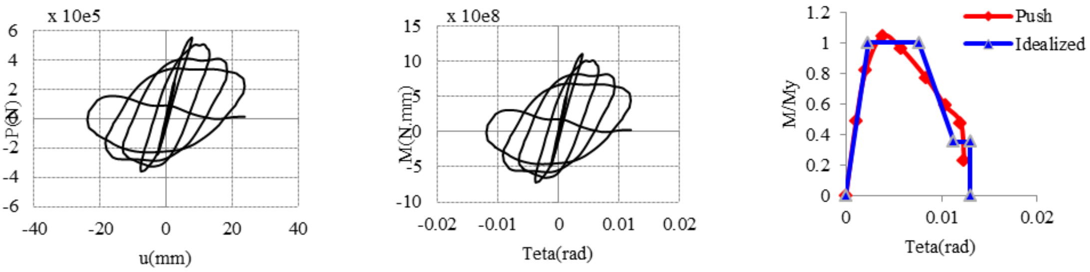

(a) (b) (c)

Fig. 17 Hysteresis curves of column model No.18 (a) Force-Displacement hysteresis curve, (b) Moment-rotation hysteresis curve and (c) Push and idealized curves

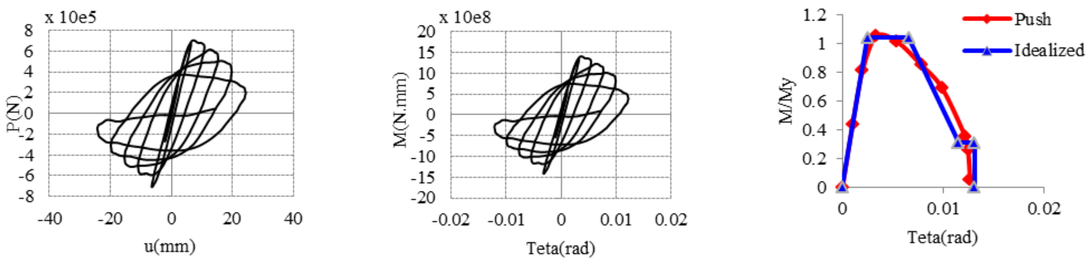

(a) (b) (c)

Fig. 18 Hysteresis curves of column model No.19 (a) Force-Displacement hysteresis curve, (b) Moment-rotation hysteresis curve and (c) Push and idealized curves

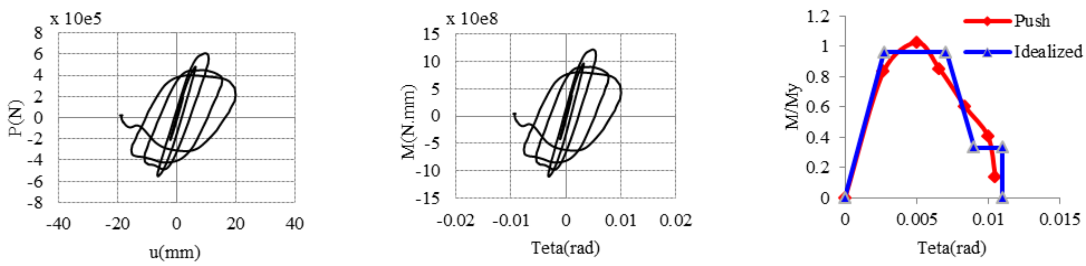

(a) (b) (c)

Fig. 19 Hysteresis curves of column model No.20 (a) Force-Displacement hysteresis curve, (b) Moment-rotation hysteresis curve and (c) Push and idealized curves